Activation of the TP53 pathway is a therapeutic vulnerability in NUP98::KDM5A^{+} pediatric AML

Luca N. Cifarelli[1-2], Hasan Issa[2], Ludovica Proietti[6], Konstantin Schuschel[2], Lucie Gack[3], Katja Menge[3], Christian Ihling[4-5], Meike Vogler[1], Andrea Sinz[4-5], Jan-Henning Klusmann[2*], Dirk Heckl[1-2*]

[1] Institute for Experimental Pediatric Hematology and Oncology, Goethe-University Frankfurt, Frankfurt am Main, Germany; [2] Dep. of Pediatrics, Goethe-University Frankfurt, Frankfurt am Main, Germany; [3] Dep. of Pediatric Hematology and Oncology, Martin-Luther-University Halle-Wittenberg, Halle, Germany; [4] Dep. of Pharmaceutical Chemistry and Bioanalytics, Martin-Luther-University Halle-Wittenberg, Halle, Germany; [5] Center for Structural Mass Spectrometry, Martin-Luther-University Halle-Wittenberg, Halle, Germany; [6] Centre of Biological Sciences, University of Veterinary Medicine, Vienna, Austria

Statement of equal author contribution

J.H.K and D.H. contributed equally to this work.

Visual abstract

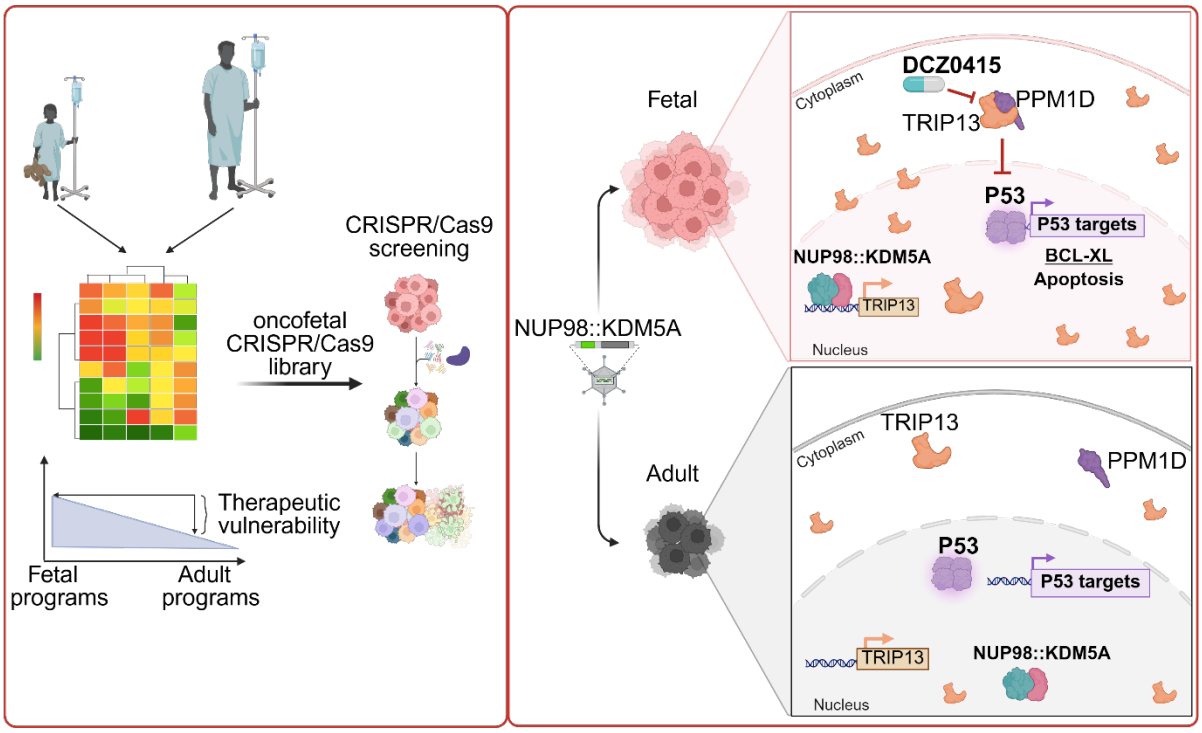

Abstract

NUP98::KDM5A–rearranged pediatric acute myeloid leukemia (AML) is a rare, infancy-predominant entity with dismal outcome and no targeted therapeutic options. Given its suspected fetal origin, we hypothesized that leukemic maintenance depends on developmentally restricted vulnerabilities embedded within fetal hematopoietic programs. Using matched fetal and adult hematopoietic stem and progenitor cell models, we integrated transcriptomic and proteomic profiling with CRISPR–Cas9 screenings to define ontogeny-specific dependencies in NUP98::KDM5A leukemia. Fetal-derived NUP98::KDM5A leukemias exhibited greater *in vivo* aggressiveness, and retained fetal transcriptional signatures compared with adult counterparts. A comparative CRISPR–Cas9 screen using a library targeting fetal gene programs, conducted in both fetal- and adult-derived NUP98::KDM5A leukemias, identified the AAA^+ ATPase TRIP13 as a selective and essential dependency in the fetal context. Mechanistically, TRIP13 physically interacted with the TP53 phosphatase PPM1D/WIP1, resulting in suppression of TP53 activation. Genetic ablation of *Trip13*, or pharmacologic inhibition using DCZ0415, a small-molecule inhibitor targeting TRIP13, reactivated TP53, induced G_2/M arrest and mitochondrial apoptosis, and depleted leukemic cells *in vitro*; these effects were fully rescued by *TP53* loss. In competitive transplantation assays, *Trip13* ablation significantly impaired leukemic fitness *in vivo*. Together, these findings define a developmentally restricted TRIP13–PPM1D–TP53 survival axis in NUP98::KDM5A AML and provide mechanistic proof-of-concept that reactivation of the TP53 signaling pathway via TRIP13 inhibition represents a therapeutically targetable vulnerability in this high-risk pediatric leukemia.

Keywords: pediatric acute myeloid leukemia; NUP98::KDM5A; fetal origin; TRIP13; PPM1D; TP53 pathway; synthetic vulnerability; targeted therapy.

46 # Introduction

47 Pediatric acute myeloid leukemia (AML) is a biologically heterogenous disease,
48 accounting for ~15-20% of childhood acute leukemias, with a mutational landscape
49 that differs substantially from adult AML and varies across pediatric age groups [1-5].
50 Increasing evidence suggests that this heterogeneity is shaped not only by genetic
51 lesions but also by the developmental stage and cellular context in which
52 transformation occurs, a concept that is particularly relevant in infant AML (≤2 years of
53 age) [6-8]. In several pediatric AML subtypes, oncogenic driver lesions can be detected
54 at birth, indicating an *in utero* origin and implicating fetal hematopoiesis as a permissive
55 developmental context for leukemic initiation [9, 10]. Although direct causal links
56 remain difficult to establish, the unique molecular properties of fetal hematopoietic cells
57 and their niche are thought to contribute to the striking enrichment of specific
58 chromosomal translocations and disease subgroups observed in early childhood.
59 Acute megakaryoblastic leukemia (AMKL) represents one such subgroup,
60 characterized by aggressive clinical behavior and inferior event-free and overall
61 survival in children without underlying Down syndrome (trisomy 21) [11-13]. Among
62 pediatric AMKLs, the chromosomal translocation t(11;12) generates the
63 NUP98::KDM5A fusion oncoprotein, composed of the N-terminal glycine-leucine-
64 phenylalanine-glycine (GLFG) repeat motif of NUP98 and the C-terminal plant
65 homeodomain finger (PHD3) domain of the histone lysine demethylase KDM5A (also
66 known as JARID1A) [14, 15]. Expression of NUP98::KDM5A potently transforms
67 murine hematopoietic stem/progenitor cells (HSPCs) and induces HOXA/B cluster
68 gene activation, recapitulating core transcriptional and phenotypic features of the
69 human disease [16-18].
70 While the fetal origin and developmental constraints of other high-risk pediatric AML
71 entities, such as *CBFA2T3::GLIS2* and *KMT2A*-rearranged leukemias, have been

extensively investigated [6], the contribution of fetal hematopoietic context to the initiation and maintenance of NUP98::KDM5A-driven leukemia remains largely unexplored [19-21]. Fetal liver HSPCs are highly proliferative and display a pronounced erythro-megakaryocytic bias, supporting rapid expansion of the lifelong hematopoietic stem cell pool through developmentally programmed epigenetic and transcriptional states, which renders them fundamentally distinct from their adult counterparts [22, 23]. These coordinated epigenetic landscapes and transcriptional programs raise the possibility that leukemias initiated in fetal hematopoiesis may remain dependent on developmentally restricted molecular circuits that are dispensable in adult cells.

Here we demonstrate that fetal hematopoietic origin markedly accelerates NUP98::KDM5A-driven leukemogenesis and enforces a critical TRIP13/PPM1D–TP53 survival axis. By exploiting this developmentally constrained dependency through genetic and pharmacologic inhibition of TRIP13, we uncover a mechanistically precise vulnerability that can be therapeutically engaged in this otherwise treatment-limited pediatric AML subtype.

Materials and methods

Cell culture

Human cell lines were purchased from the German Collection of Microorganisms and Cell Cultures (DSMZ) and maintained according to the supplier's instructions. Fetal HSPCs were obtained from the MRC-Wellcome Trust Human Developmental Biology Resource (HDBR). Pediatric AML samples were collected from patients enrolled in the AML Berlin-Frankfurt-Münster treatment protocols for children and adolescents. The study was approved by the institutional review boards of all participating centers. All investigations were performed in accordance to the Declaration of Helsinki and local

97 laws and regulations, and informed consent was obtained from all patients and
98 custodians.
99 Human and murine HSPCs were prepared and cultured as previously described and
100 maintained for at least 60 days [24, 25].
101 Media promoting the megakaryocyte differentiation of HSPCs consisted of respective
102 media supplemented with corresponding cytokines: 15ng/mL SCF/Scf and 15ng/mL
103 TPO/Tpo. All cytokines were purchased from Peprotech.
104 mFL-HSPCs were cultured in pre-stimulation medium composed by: DMEM
105 supplemented with 10% FBS, 1% penicillin/streptomycin, 1% sodium pyruvate, 1% L-
106 glutamine, 1% nonessential amino acids, 25ng/mL murine TPO and 25ng/mL murine
107 SCF.
108 mBM-HSPCs were cultured in pre-stimulation medium composed by: IMDM
109 supplemented with 10% FBS, 1% penicillin/streptomycin, 1% sodium pyruvate, 1% L-
110 glutamine, 1% nonessential amino acids, 50ng/mL murine TPO and 50ng/mL murine
111 SCF.
112 After 24 hours post-transduction, mFL-HSPCs and mBM-HSPCs were cultured in
113 selection medium promoting megakaryocytic differentiation composed by: DMEM and
114 IMDM, respectively, supplemented with 10% FBS, 1% penicillin/streptomycin, 1%
115 sodium pyruvate, 1% L-glutamine, 1% nonessential amino acids, 15ng/mL murine Tpo
116 and 15ng/mL murine Scf.
117 Human fetal and adult PB CD34+ HSPCs: cells were cultured in pre-stimulation
118 medium composed by: Stemspan SFEM II supplemented with 1%
119 penicillin/streptomycin, 0.75 μM Stemregenin, 35nM UM171, 100ng/ml human FLT3L,
120 50ng/ml human TPO, 100ng/ml human SCF, 20ng/ml human IL6. After 24 hours post-
121 nucleoporation, hFL-HSPCs and adult PB CD34+ HSPCs cells were cultured in
122 selection medium promoting megakaryocytic differentiation composed by: Stemspan

123 SFEM II, respectively, supplemented with 10% FBS, 1% penicillin/streptomycin,
124 15ng/mL human TPO and 15ng/mL human SCF.

125 **Lentiviral vector construction and production**

126 Lentiviral particles were generated by co-transfecting HEK293T cells with the
127 corresponding expression constructs. pMD2.G and psPAX2 (Addgene #12259 and
128 #12260), via the polyethyleneimine transfection method as previously described [26,
129 27]. Codon-optimized cDNAs were similarly cloned into the same SIN40C.SFFV
130 backbone encoding GFP or dTomato as a fluorescent reporter [24, 25]. For inducible
131 expression, a doxycycline-inducible SIN40C.TRE vector was used [25]. All plasmids
132 generated in this study have been deposited at Addgene and are listed in
133 Supplementary Table 1.
134 A list of sgRNAs is in Supplementary Table 2 (designed using CCTop online tools [28])
135 that have been cloned into the SGL40C.EFS.E2Crimson or SGL40C.EFS.dTomato
136 vectors (Addgene #100894 and #89395) [29].
137 NUP98::KDM5A encoding cDNA was designed based on a report in human patients
138 [30]. TRIP13-encoding cDNA was designed based on Ensembl genome browser. All
139 cDNAs were tagged at the 5' terminus with three HemoAgglutinin tag (3xHA), flanked
140 with AgeI at 5' terminus and MluI at 3' terminus, codon optimized and ordered from
141 pTwistAmp.
142 Plasmids were retransformed and cDNAs were subcloned using the restriction
143 enzymes AgeI and MluI into the backbone vectors for constitutive expression:
144 NUP98::KDM5A cDNA in SIN40C.SFFV.GFP.IRES.MCS and TRIP13 in cDNA in
145 SIN40C.SFFV.MCS.IRES.dtomato and in
146 SIN40C.TRE.MCS.IRES.dTomato.PGK.sfGFP.P2A.Tet3G.

147 **Transduction**

148 Cells were transduced with concentrated viral particles in the presence of 2-5µg/ml
149 polybrene as previously described [24, 25, 31]. Primary human and murine HSPCs
150 were transduced in Retronectin-coated plates according to manufacturer's instructions
151 (Takara Bio) as previously described [31].

152 **CRISPR/Cas9 library screening**

153 15 x 10^6 fetal and adult NUP98::KDM5A$^+$, FPD-AML and ML-DS models were
154 lentivirally transduced with the fetal signature sgRNA library (MOI=0.3) to achieve
155 sufficient representation (1000-fold coverage per sgRNAs). Samples were harvested
156 at 2 days post-transduction and at 16 population doublings, corresponding to
157 approximately 30 days of culture. Genomic DNA was isolated as previously described
158 [24].
159 704 genes of our CRISPR-Cas9 library, targeting the TP53 pathway, were collected
160 using publicly available GSEA gene sets.
161 Model-based analysis of genome-wide CRISPR/Cas9 knockout (MAGeCK) [32] was
162 used to identify hits from the sgRNA screen. Double barcoded reads were
163 demultiplexed using custom R scripts; guides with fewer than 20 reads in ≥75% of all
164 samples were excluded. Raw read counts were passed to the MAGeCK test command
165 using default parameters. Samples collected at the endpoint were compared to day 2
166 to determine negative enrichment. Genes with a P-value <0.05 as determined by
167 MAGeCK were deemed significant.

168 **Proliferation and rescue assays**

169 To evaluate the effect of NUP98::KDM5A transformation, mFL-HSPCs and mBM-
170 HSPCs were co-transduced with lentiviral vectors overexpressing the human cDNA
171 encoding NUP98::KDM5A, which was assigned to a green fluorescent protein thereby
172 allowing direct clonal growth competition.

173 To assess growth advantages conferred by overexpression of sgRNA(s) or TRIP13
174 cDNA and for rescue experiments, transduced mFL-HSPCs were measured every 2/3
175 days starting 72 hours post-transduction and analyzed for reporter gene expression.
176 For inducible expression of TRIP13, doxycycline was added to culture medium at a
177 concentration of 0.5 µg/mL 96 hours post transduction.

178 **Flow cytometry and sorting**

179 To assess the expression of fluorescent reporter protein and their immunophenotype,
180 cells were analyzed for the expression of surface cell markers using fluorochrome-
181 coupled antibodies, listed in Supplementary Table 1. The following panels were used:
182 Myeloid (CD11b and Gr-1), Progenitor (CD34, CD16/32, C-kit/CD117, Sca-1),
183 Megakaryocytic (CD41, CD42d) Erythroid (CD71 and CD235a for human cells or
184 Ter119 for murine cells). Flow cytometry was performed on a CytoFLEX flow cytometer
185 (Beckman Coulter) and the data analysis was done using Kaluza 1.5 (Beckman
186 Coulter) software.
187 The same procedure was performed to sort the cell subpopulation of interest. Cells
188 were sorted using BD FACSAria™ II Flow Cytometer (BD Biosciences).
189 Apoptotic cell death and cell cycle analysis was performed as previously described
190 [25].

191 **Micrographs**

192 Micrographs were obtained with a Keyence BZ-9000 Microscope using the BZ-II
193 viewer and images were processed with the BZ-II Analyzer software.

194 **Drug response assays**

195 For drug response curves using DCZ0415 (MedChemExpress), cell viability was
196 assessed using the CellTiter-Glo® Cell Viability Assay (Promega) according to the
197 manufacturer's instructions after 2-5-7 days post-treatment.

198 Synergy plots, summary Bliss score calculations were generated and performed with
199 SynergyFinder [33]. All conditions were normalized to DMSO treated control. Data
200 represent the mean ± SD of biological triplicates.

201 **Proteomic analysis**

202 Total cell lysis and Western blotting were performed as previously described [24, 25].
203 Blots were developed using Amersham™ ECL Prime Western Blotting Detection
204 Reagent (Thermo Fisher Scientific).
205 Co-immunoprecipitation of TRIP13 was performed on OCI-AML3 cells using Anti-HA
206 antibody coupled to magnetic beads (Pierce Anti-HA Magnetic Beads). After cell lysis
207 and affinity pulldown, proteins were processed as previously described [24, 25].

208 **Gene expression profiling**

209 NUP98::KDM5A and control (EV) transduced mFL-HSPCs and mBM-HSPCs were
210 FACS-sorted 3, 21 days after transduction; sgLuc- and sgTrip13- transduced mFL-
211 HSPCs expressing NUP98::KDM5A translocation were FACS-sorted 4 days after
212 transduction. Fetal NUP98::KDM5A cells were treated with DCZ0415 or DMSO control
213 24h prior gene expression profiling. RNA was extracted using the Quick-RNA
214 Microprep Kit (Zymo Research) as previously described [25]. A minimum amount of
215 150ng RNA was used as input material for the RNA sample preparations. RNA-
216 sequencing was performed by Novogene Company, Ltd. Sequencing libraries were
217 generated and sequenced as previously described [25].
218 Raw FASTQ data (raw reads) were first pre-processed using fastp [34] and then further
219 processed as previously described [35]. Differential expression analysis was
220 performed using the DESeq2 package in R [36]. The resulting P-values were adjusted
221 using the Benjamini and Hochberg's approach for controlling the False Discovery Rate
222 (FDR) [37]. Genes with an adjusted P-value <0.05 were considered differentially
223 expressed.

224 Gene set enrichment analysis (GSEA) was performed using the Broad GSEA software
225 [38, 39] with the permutation type set to “Gene_set” (1000 permutations). Human gene
226 symbols were mapped to murine gene symbols using orthologue annotations provided
227 by Ensembl [40] considering only one-to-one orthologue relationships.

228 **Animal studies**

229 All experiments involving mice were performed in accordance with protocols approved
230 by the local authorities (Landesverwaltungsamt Sachsen-Anhalt).
231 B6J.129 (Cg)-Gt(ROSA)26Sortm1.1(CAG-cas9*.-EGFP)Fezh/J) (Jackson Laboratory.
232 RRID: IMSR_JAX:026179) and C57BL/6J (Charles River. RRID: IMSR_JAX:000664)
233 mice were maintained in a specific pathogen-free environment in individual ventilated
234 cages and fed with autoclaved food and water at the Martin-Luther-University Halle-
235 Wittenberg.

236 **Transplantations and analysis of leukemic mice**

237 2 x 10^6 cells were injected intravenously into sublethally irradiated (7 Gy) C57BL/6N
238 mice. Engraftment of the transplanted cells was evaluated by tail bleeding of the
239 recipients every 4 weeks. When signs of disease occurred, the mice were sacrificed
240 and harvested bone marrow cells were stained with the following fluorochrome-
241 coupled antibodies describe above.

242 **Statistical analysis**

243 All statistical analyses were performed with GraphPad Prism 8 (San Diego, CA).
244 Unless indicated otherwise, 2-tailed Student´s t-tests were used to determine the P-
245 value between 2 groups. Statistical analyses of experiments were performed with
246 analysis of variance (ANOVA) with Bonferroni *post hoc* analysis for comparisons
247 between ≥3 groups. Kaplan-Meier method was used to determine mice survival using

248 log-rank (Mantel-Cox) tests for statistical analyses. *P, .05, **P, .01, ***P, .001, ****P,
249 .0001. A value of P, .05 was considered statistically significant.
250 All statistical tests and sample numbers are disclosed in the respective figure legends
251 and supplemental tables.

252 Results

253 NUP98::KDM5A induces highly aggressive leukemia in fetal HSPCs

254 To investigate whether the developmental origin of the leukemia initiating cell is an
255 accelerator of NUP98::KDM5A-driven leukemogenesis, we established matched fetal
256 and adult murine leukemia models. We transduced murine hematopoietic stem and
257 progenitor cells (HSPCs) from fetal liver at embryonic day 13.5 (mFL-HSPCs) and from
258 adult bone marrow (mBM-HSPCs) with a lentiviral vector expressing human
259 NUP98::KDM5A cDNA [30] (Fig. 1a). Both fetal- and adult-derived HSPCs exhibited
260 progressive expansion of NUP98::KDM5A^{+} cells, whereas control vector–transduced
261 cells exhausted over time, indicating efficient leukemic transformation in both
262 developmental contexts (Fig. 1b and Supplementary Fig. 1a). However, despite
263 comparable transduction efficiencies and similar baseline immunophenotype, fetal-
264 derived NUP98::KDM5A^{+} cells expanded significantly faster than their adult
265 counterparts, consistent with an ontogeny-dependent increase in leukemic fitness (Fig.
266 1b and Supplementary Fig. 1a).

267 Immunophenotypic analysis showed that NUP98::KDM5A expression maintained cells
268 in a highly immature LSK (Lineage^{-} c-Kit^{+} Sca1^{+}) state with marked maturation arrest,
269 findings that were corroborated by transcriptional profiling (Fig. 1c, Supplementary Fig.
270 1b-c and Supplementary Table 3). Gene expression analysis further revealed that fetal
271 NUP98::KDM5A^{+} cells retained transcriptional signatures associated with fetal

272 hematopoietic origin compared to adult-derived cells, highlighting the influence of
273 developmental origin on leukemic phenotype and aggressiveness (Fig. 1d and
274 Supplementary Table 4). Consistent with patient samples, both models exhibited
275 upregulation of *HOXA* and *HOXB* gene clusters, together with marked downregulation
276 of *RB1* target genes (Supplementary Fig. 1c and Supplementary Table 3), resembling
277 a transcriptional program of the RB1-mutant state frequently associated with
278 NUP98::KDM5A AML [12, 15, 41].

279 *In vivo*, transplantation of fetal NUP98::KDM5A^{+} cells into syngeneic recipients
280 resulted in significantly accelerated leukemia onset compared to adult-derived cells
281 (median disease-free survival: fetal 36 days versus adult 70 days; log-rank $P = 1.07 \times$
282 10^{-5}; Fig. 1e). Splenomegaly was significantly more pronounced in mice transplanted
283 with fetal NUP98::KDM5A^{+} cells (Fig. 1f). Leukemic blasts in the bone marrow
284 expressed high levels of the mature myeloid surface marker Gr-1 and CD11b (Mac-1),
285 together with persistence of an immature LSK population (Supplementary Fig. 1d-e).

286 Collectively, these data demonstrate that developmental origin is a major determinant
287 of NUP98::KDM5A-driven leukemic aggressiveness, with fetal hematopoietic cells
288 providing a permissive context that accelerates disease onset and progression.

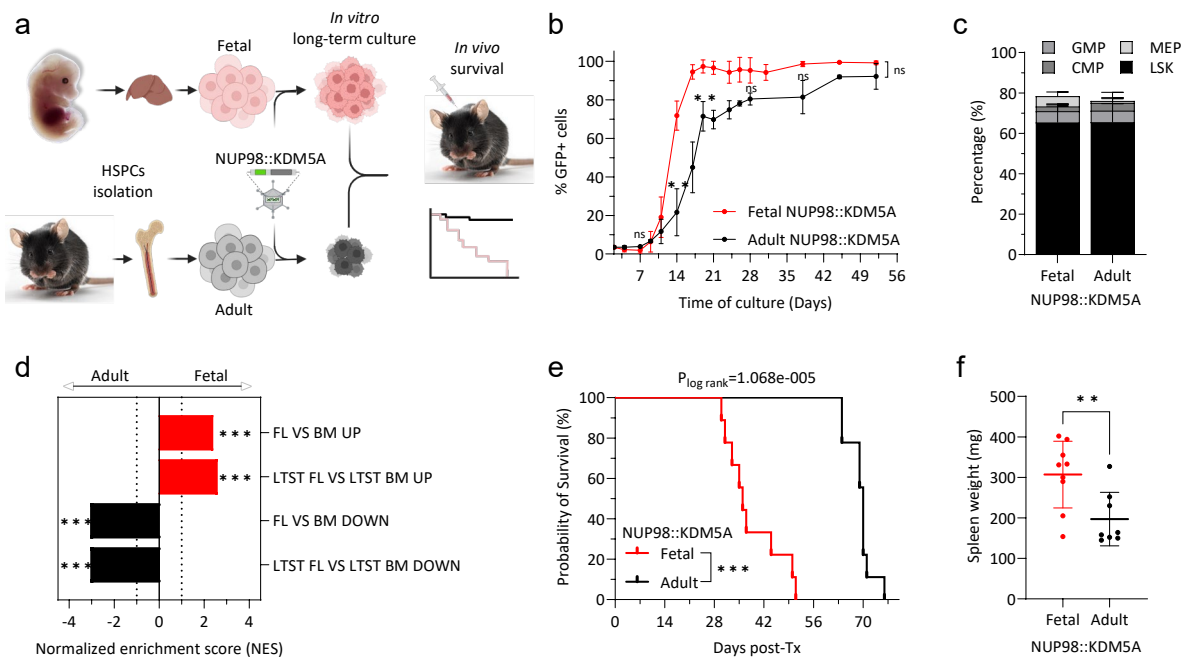

Fig. 1. NUP98::KDM5A fusion oncoprotein induces a more aggressive disease in fetal cells.

a) Schematic workflow for the generation of in vitro and in vivo murine models of constitutive overexpression of NUP98::KDM5A fusion oncoprotein in murine Hematopoietic Stem and Progenitor Cells (HSPCs) isolated from fetal liver (mFL-HSPCs) of healthy fetuses at E13.5 and bone marrow of adult mice (mBM-HSPCs). Created in Biorender.com

b) GFP+ percentage of fetal and adult NUP98::KDM5A+ cells maintained in liquid culture. Data from 1 representative experiment performed in replicates (n > 3) are shown as mean s.d. (t-test).

c) Bar graph showing the percentage of LSK (Lineage negative, c-kit+ and Sca1+), Megakaryocytic-erythroid (MEP; Lineage negative, c-kit+, Sca1-, CD16/CD32- and CD34+) and common myeloid (CMP; Lineage negative, c-kit+, Sca1-, CD16/CD32- and CD34-) and granulocyte/monocyte (CMP; Lineage negative, c-kit+, Sca1-, CD16/CD32+ and CD34+) progenitors of fetal and adult NUP98::KDM5A+ cells after 4 weeks of culture. (mean ± s.d., n > 3)

d) Bar graphs showing the normalized enrichment scores (NES) of significantly upregulated or downregulated gene sets in fetal NUP98::KDM5A^{+} cells compared to adult NUP98::KDM5A^{+} cells.

e) Kaplan-Meier survival curves of C57BL/6N mice transplanted with fetal and adult NUP98::KDM5A^{+} cells (n ≥ 6).

f) Dot plot showing spleen weights of C57BL/6N mice transplanted with fetal and adult NUP98::KDM5A^{+} cells (mean ± s.d., n ≥ 6) (t-test).

ns, not significant * P < .05, ** P < .01, ***P < .001, ****P < .0001

313 **Fetal dependency screening reveals TRIP13 as a critical vulnerability in**
314 **NUP98::KDM5A$^+$ AML**

315 The aggressive phenotype of fetal-derived NUP98::KDM5A leukemia is closely linked
316 to the persistence of fetal transcriptional programs, which remained active in a post-
317 fetal hematopoietic environment. We reasoned that such developmentally regulated
318 programs might impose context-specific dependencies required for leukemic
319 maintenance and therefore represent a potential therapeutic vulnerability. To identify
320 these dependencies, we performed a CRISPR-Cas9 loss-of-function screen targeting
321 867 genes, overexpressed in both human and murine fetal liver HSPCs compared to
322 their adult counterparts [42], in fetal- and adult-derived NUP98::KDM5A$^+$ leukemia
323 models (Fig. 2a-b). To distinguish NUP98::KDM5A- and fetal-specific dependencies
324 from broader AML requirements, we complemented these screens with two additional
325 murine AML models: familial-platelet disorder with predisposition to AML (FPD-AML,
326 loss of *Runx1* and *Bcor*) [43], and myeloid leukemia in Down syndrome (ML-DS) (Fig.
327 2c and Supplementary Fig. 2a) [24, 31, 44]. Applying a depletion threshold of >70%
328 identified seven candidates, with the the AAA+ ATPase (ATPases Associated with
329 diverse cellular Activities) *Trip13* displaying the highest fetal-to-adult dependency ratio
330 (Supplementary Fig. 2b). The effect of *Trip13* knock-out was subsequently validated in
331 a single-well fluorescence-based depletion assay using independent sgRNAs,
332 confirming robust on-target effects (Fig. 2d). To corroborate these findings in a human
333 system, we performed CRISPR-based *TRIP13* knock-out in a panel of human leukemic
334 and non-leukemic (HT1080) cell lines, and primary human fetal HSPCs expressing
335 NUP98::KDM5A. Consistent with the murine results, *TRIP13* loss markedly impaired
336 the growth of NUP98::KDM5A$^+$ human fetal HSPCs, whereas most control cell lines
337 showed only modest proliferation defects (Fig. 2e). Gene expression analyses further
338 demonstrated that *TRIP13* is upregulated as part of a fetal transcriptional program,

339 with higher expression in fetal compared to adult HSPCs, and in pediatric AMKL
340 relative to adult HSPCs and mature hematopoietic populations (Fig. 2f). Notably, the
341 NUP98::KDM5A fusion oncoprotein not only maintained but further increased *TRIP13*
342 expression in fetal but not in adult cells, indicating a fetal context-specific effect of the
343 fusion on *TRIP13* regulation (Fig. 2g).

344 Collectively, these data identify *TRIP13* as a fetal context-dependent vulnerability in
345 NUP98::KDM5A^{+} leukemias, supporting its prioritization for mechanistic and
346 therapeutic interrogation in this high-risk AML subtype.

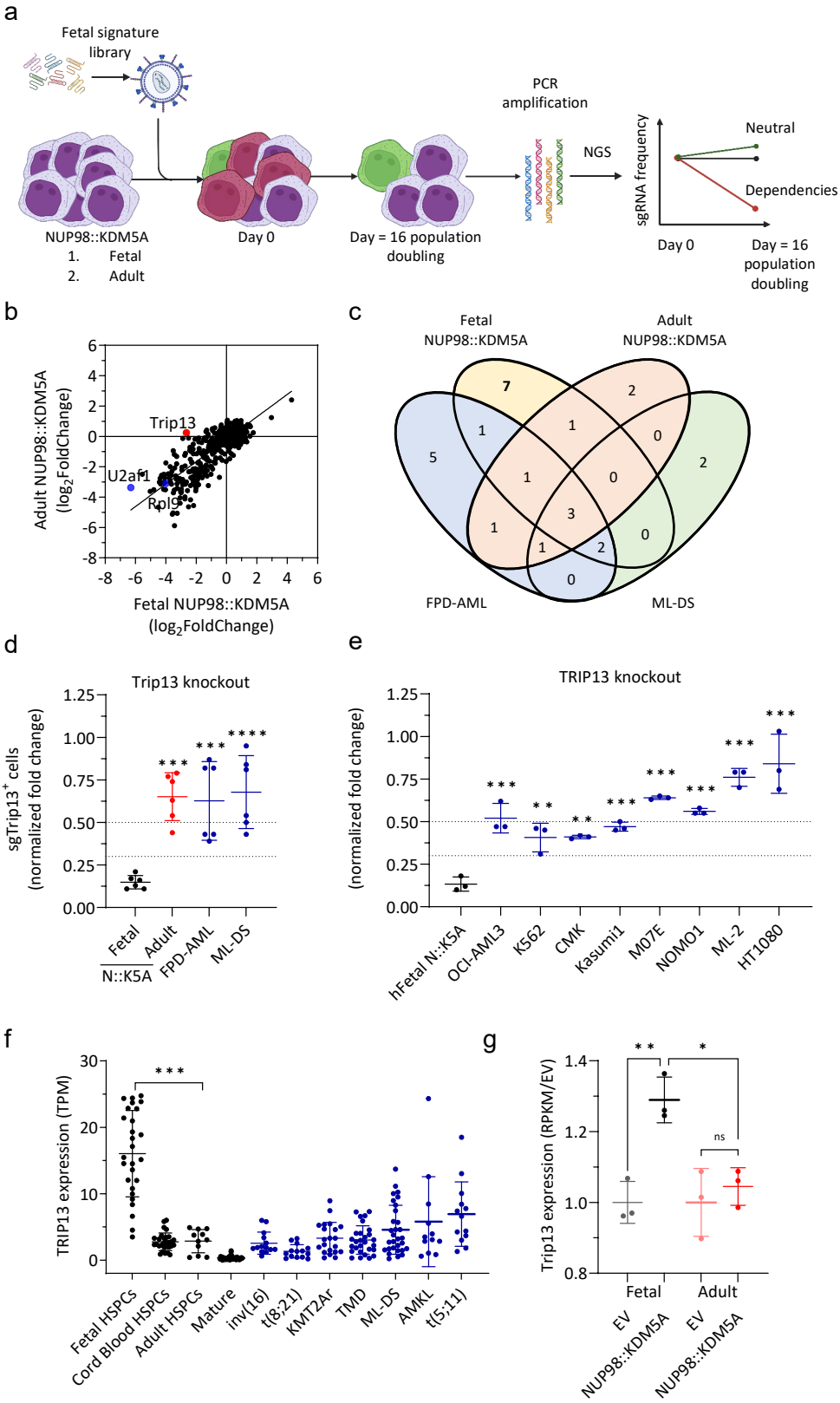

Fig. 2. CRISPR-Cas9 knock-out screening reveals *TRIP13* dependency in fetal NUP98::KDM5A⁺ model.

a) Schematic workflow of the high-throughput fetal signature-based CRISPR-Cas9 *in vitro* screen.

352 b) Dot plots showing the log2 fold change of the fetal enriched genes targeted by sgRNAs in
353 fetal (x-axis) and adult (y-axis) NUP98::KDM5A$^+$ models. Blue dots represent positive
354 control (*Rpl9*, *U2af1*). Red dots represent selected candidate gene *Trip13*. (n =2)
355 c) Venn diagram illustrating significantly (P-value < 0.05) depleted (depletion > 70%) sgRNAs
356 in different murine leukemia models.
357 d) Dot plot showing the percentage of *Trip13*-targeting sgRNA-transduced fetal, adult
358 NUP98::KDM5A$^+$ (N::K5A), FPD-AML and ML-DS models after 21 days of culture,
359 normalized to (negative control sgRNA [sgCtr]) and to day 2 (mean ± s.d., n > 3 per sgRNA,
360 1-way ANOVA).
361 e) Dot plot showing the percentage of *TRIP13*-targeting sgRNA-transduced hFL
362 NUP98::KDM5A$^+$ (N::K5A) cells and leukemia cell lines (OCI-AML3; K562; CMK; Kasumi1;
363 M07E; NOMO1; ML-2) and non-leukemia cell line (HT1080) after 21 days of culture,
364 normalized to (negative control sgRNA [sgCtr] and positive control sgRNA [sgRPL9 and
365 sgU2AF1]) and to day 2 (mean ± s.d., n = 3 per sgRNA, 1-way ANOVA).
366 f) Dot plot showing the expression of *TRIP13* in subgroups of HSPCs and pediatric AML from
367 the HemAtlas dataset.
368 g) Dot plot showing the expression of *Trip13* in control (EV) or NUP98::KDM5A$^+$ murine fetal
369 and adult cells after 21 days of culture (n = 3).
370 ns, not significant * P < .05, ** P < .01, ***P < .001, ****P < .0001.

371 **Trip13 loss triggers TP53-dependent apoptosis**

372 To further confirm that *Trip13* loss was causative for the observed growth defect, we
373 co-transduced fetal NUP98::KDM5A$^+$ cells with *TRIP13* cDNA together with *Trip13*-
374 targeting sgRNAs. *TRIP13* overexpression fully rescued cell depletion, demonstrating
375 on-target specificity of *Trip13* disruption (Fig. 3a). *Trip13* knock-out was confirmed by
376 Western blotting (Supplementary Fig. 3a), and resulted in a marked increase in
377 apoptosis (Fig. 3b) and a G_2/M cell-cycle arrest (Fig. 3c), consistent with the
378 established role of TRIP13 in mitotic checkpoint control [45]. *Trip13* loss did not alter
379 the differentiation status of leukemic cells, as assessed by immunophenotypic analysis
380 (Supplementary Fig. 3b).

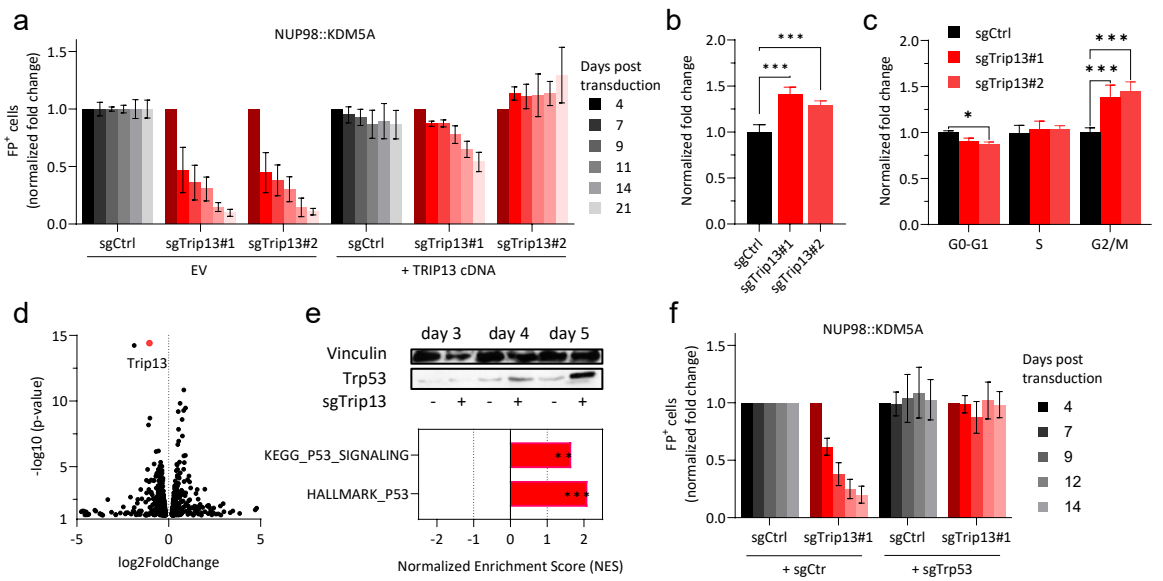

Fig. 3. *Trip13* loss activates the TP53 pathway and arrests fetal NUP98::KDM5A⁺ cell proliferation.

a) Bar plot showing the percentage of sgRNA-transduced (negative control sgRNA [sgCtr], sgTrip13#1-2) empty vector (EV) and TRIP13 overexpressing fetal NUP98::KDM5A⁺ cells after 14 days of culture, normalized to day 4 (mean±s.d., n > 3 per sgRNA, 1-way ANOVA)

b) Bar graphs showing the percentage of Annexin-V⁺ sgRNA-transduced (negative control sgRNA [sgCtr], sgTrip13#1-2) fetal NUP98::KDM5A⁺ cells after 5 days of culture, normalized to control sgRNA (sgCtr) (mean ± s.d., n > 3 per sgRNA, 1-way ANOVA).

c) Bar plot showing the percentage of sgRNA-transduced (negative control sgRNA [sgCtr], sgTrip13#1-2) fetal NUP98::KDM5A⁺ cells in G0-G1, S and G2/M phase after 5 days of culture (mean ± s.d., n > 3 per sgRNA, 2-way ANOVA).

d) Volcano plot showing the differentially expressed genes upon *Trip13* knock-out in fetal NUP98::KDM5A⁺ cells P-value < 0.05 (n = 3). RNA-seq-based gene expression analysis of sgRNA-transduced (negative control sgRNA [sgCtr], sgTrip13#1) fetal NUP98::KDM5A⁺ cells was performed after 4 days of culture.

e) Timeline Western blot showing TP53 protein levels in sorted sgRNA-transduced (negative control sgRNA [Luc], sgTrip13#1) fetal NUP98::KDM5A⁺ cells 4 days after transduction. Endogenous Vinculin was used as loading control.
Bar graphs showing the normalized enrichment scores (NES) of significantly deregulated gene sets associated with TP53 pathway in *Trip13* knock-out fetal NUP98::KDM5A⁺ cells compared to control sgRNA.

f) Bar plot showing the percentage of sgRNA-transduced (negative control sgRNA [sgCtr], sgTrip13, sgTrp53) fetal NUP98::KDM5A⁺ cells after 14 days of culture, normalized to day 4 (mean±s.d., n > 3 per sgRNA, 1-way ANOVA)

406 ns, not significant * P < .05, ** P < .01, ***P < .001, ****P < .0001.

407 To define the mechanism underlying *Trip13* dependency, we profiled transcriptomic
408 changes four days after CRISPR-Cas9-mediated *Trip13* deletion in fetal
409 NUP98::KDM5A$^+$ cells (Fig. 3d). Gene set enrichment analysis (GSEA [38]) revealed
410 a striking and selective enrichment of TP53 signaling pathway signatures upon *Trip13*
411 loss (Fig. 3e and Supplementary Fig. 3c, Supplementary Table 5). In line with this
412 transcriptional response, TP53 protein levels increased in a time-dependent manner
413 after *Trip13* knock-out (Fig. 3e). Importantly, concomitant deletion of *Trp53* rescued
414 the growth defect induced by *Trip13* loss (Fig. 3f), demonstrating that TP53 activation
415 is required for the *Trip13*-dependent loss of leukemic cell fitness in fetal
416 NUP98::KDM5A$^+$ AML cells. Given the reported role of TRIP13 in DNA damage repair
417 [46, 47], we next examined whether TP53 activation resulted from increased genotoxic
418 stress. Although leukemic cells exhibited baseline γH2AX positivity, *Trip13* deletion did
419 not further augment γH2AX levels compared with controls (Supplementary Fig. 3d),
420 arguing against DNA damage-accumulation as the primary trigger of TP53 activation
421 in this context.

422 Together, these results establish that fetal *NUP98::KDM5A*$^+$ AML cells are sensitive to
423 TP53 activation and that *Trip13* sustains leukemic survival by suppressing TP53
424 activity, without requiring increased DNA damage signaling.

425 **TRIP13 interacts with PPM1D/WIP1 to repress TP53 pathway activation**

426 To elucidate how TRIP13 regulates TP53 activity, we next mapped TRIP13 protein-
427 protein interaction network using co-immunoprecipitation followed by mass
428 spectrometry (IP-MS). Doxycycline-inducible hemagglutinin (HA)-tagged TRIP3 was
429 expressed in a TP53 wild-type leukemia cell line (OCI-AML3) (Fig. 4a) [48, 49]. Among
430 the proteins identified by TRIP13 pull-down, we focused on 33 candidates previously

431 annotated in the STRING interaction database to be functionally or physically
432 connected to TP53 (Fig. 4b). To prioritize TRIP13-associated complexes and identify
433 the key mediators of TP53 suppression, we reasoned that the loss of a critical TRIP13
434 interactor would phenocopy *Trip13* deletion. Specifically, we predicted that disruption
435 of such an interactor would induce TP53-dependent depletion of fetal NUP98::KDM5A$^+$
436 cells, a phenotype reversible by concomitant *Trp53* deletion. Consistent with this
437 hypothesis, CRISPR-mediated knock-out of 16 of the 33 candidate interactors resulted
438 in a depletion pattern similar to that observed following *Trip13* knock-out
439 (Supplementary Fig. 4a), which could be rescued by *Trp53* knock-out in 6 of the 16
440 TRIP13-associated candidates (Supplementary Fig. 4b). Among those 6 interactors,
441 the protein phosphatase PPM1D/WIP1, a well-known regulator of TP53, emerged as
442 the top candidate fulfilling both criteria: induction of leukemic cell depletion upon loss
443 and rescue of this phenotype by *Trp53* co-deletion (Fig. 4c and Supplementary Fig.
444 4b). PPM1D/WIP1 is a well-established regulator of TP53 signaling, acting both directly
445 and indirectly, including stabilization of MDM2 [50]. Co-immunoprecipitation followed
446 by Western blotting confirmed a physical interaction between TRIP13 and
447 PPM1D/WIP1 (Fig. 4d), and consistent with a functional interaction, deletion of either
448 *Trip13* and *Ppm1d* in fetal NUP98::KDM5A$^+$ cells resulted in increased TP53 protein
449 levels (Fig. 4e). Notably, *PPM1D/WIP1* expression, similar to *TRIP13*, was elevated in
450 pediatric AMKL patients compared to adult HSPCs and mature hematopoietic cells
451 (Supplementary Fig. 4c), supporting the relevance of this regulatory axis in pediatric
452 disease.

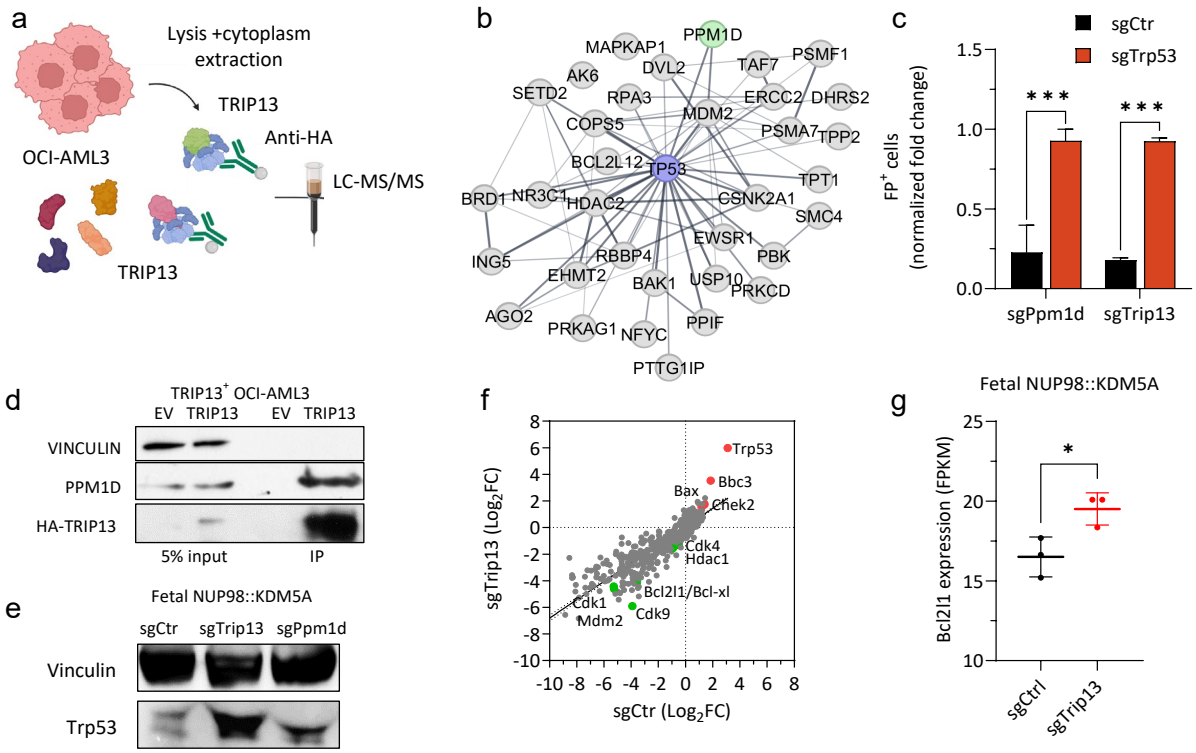

Fig. 4 TRIP13 interacts with PPM1D/WIP1 to repress the TP53 pathway.

a) Experimental workflow for isolating HA-tagged TRIP13 protein and its interactors from OCI-AML3 cells.

b) String protein-protein interaction network of 33 TRIP13-interacting candidates. Network nodes (colored circles) represent proteins, lines between the nodes (edges) indicate the different types of interaction (functional and physical protein associations), the line thickness indicates the confidence of interaction (0.4).

c) Bar plot showing the percentage of sgRNA-transduced (sgPpm1d, sgTrip13) fetal NUP98::KDM5A^{+} cells in combination with negative control sgRNA [sgCtr] or sgTrp53 after 14 days of culture, normalized to day 2 (mean±s.d., n > 3 per sgRNA, 1-way ANOVA) .

d) Western blot showing co-immunoprecipitation of PPM1D after HA-pulldown of HA-tagged TRIP13 in OCI-AML3 cells. Endogenous Vinculin was used as loading control.

e) Western blot showing TP53 protein levels in sorted sgRNA-transduced (negative control sgRNA [Luc], sgTrip13 and sgPpm1d) fetal NUP98::KDM5A^{+} cells 4 days after transduction. Endogenous Vinculin was used as loading control.

f) Dot plots showing the log2 fold change of the TP53 pathway-related genes targeted by control (x-axis), *Trip13*-depleted (y-axis) fetal NUP98::KDM5A^{+} cells. Red and green dots represent selected candidate genes. (n = 2)

g) Dot plot showing the expression of *Bcl2l1* of control or *Trip13*-depleted fetal NUP98::KDM5A^{+} cells after 4 days of culture (n = 3).

ns, not significant * P < .05, ** P < .01, ***P < .001, ****P < .0001.

475 To further position TRIP13 within the TP53 signaling network, we performed a
476 CRISPR-Cas9 knock-out screen targeting 704 TP53 pathway-associated genes in
477 fetal NUP98::KDM5A^{+} cells, in the presence or absence of *Trip13* deletion (Fig. 4f).
478 This approach enabled systematic identification of genetic modifiers that either
479 mitigated or exacerbated the growth defect induced by *Trip13* loss.
480 In addition to Trp53 depletion, knock-out of the checkpoint kinase *Chek2* and the pro-
481 apoptotic effector *Bax* were selectively rescued by *Trip13*-deficiency, indicating
482 engagement of a CHEK2–TP53–BAX mitochondrial apoptotic pathway, which was
483 further supported by a rescue of the *Trip13* loss by depletion of the TP53-induced BH3-
484 only protein *Bbc3/Puma* (Fig. 4f), and an upregulation of *Bbc3/Puma* mRNA upon
485 *Trip13* loss (Supplementary Fig. 4d).
486 Conversely, loss of several negative regulators of TP53 signaling further enhanced the
487 antiproliferative effects of *Trip13* deletion. In particular, knock-out of *Mdm2* and *Bcl-*
488 *xl/Bcl2l1* synergized with *Trip13* loss, consistent with cooperative derepression of TP53
489 activity and reinforcement of apoptotic signaling (Fig. 4f). Notably, *Bcl2l1/Bcl-xl* mRNA
490 expression was also increased following *Trip13* deletion, suggesting engagement of
491 compensatory survival feedback mechanisms downstream of TP53 activation (Fig.
492 4g).
493 In addition to core TP53 regulators, several genes involved in cell-cycle progression
494 and transcriptional control exhibited enhanced depletion specifically in *Trip13*-deficient
495 cells, including *Cdk1*, *Cdk4*, *Cdk9*, and *Hdac1*, identifying context-specific co-
496 dependencies that emerge under conditions of *Trip13*-loss initiated TP53 signaling
497 (Fig. 4f).
498 Collectively, these genetic interaction data frames a model in which *TRIP13* restrains
499 TP53 pathway activation through PPM1D/WIP1 and downstream regulators, thereby
500 preventing engagement of a CHEK2–BAX–dependent mitochondrial apoptotic

program. Consequently, loss of *TRIP13* unmasks a potent TP53-centered vulnerability in fetal NUP98::KDM5A$^+$ leukemia cells that is further modulated by regulators of apoptosis, cell-cycle progression, and transcriptional control.

Therapeutic Targeting of TRIP13 Reactivates TP53 in NUP98::KDM5A$^+$ AML

Our combined proteomic and genomic analyses identified TRIP13 as a critical suppressor of TP53 in fetal NUP98::KDM5A$^+$ AML, raising the possibility that pharmacological inhibition of TRIP13 could be therapeutically exploitable [51]. To test this, we treated leukemic cells with DCZ0415, a small-molecule inhibitor of TRIP13. DCZ0415 phenocopied genetic *Trip13* loss and robustly induced apoptosis in NUP98:KDM5A$^+$ cells in a dose-dependent manner (mean IC_{50} fetal = 22 µM, adult = 26 µM). NUP98::KDM5A$^+$ cells were significantly more sensitive to DCZ0415 than control leukemia models, including FPD-AML and ML-DS, as well as normal adult bone marrow HSPCs (mean IC_{50}: FPD-AML: 50 µM, ML-DS: 35 µM, mBM-HSPCs: 45 µM) (Fig. 5a and Supplementary Fig. 5a-b). Human fetal NUP98::KDM5A$^+$ cells exhibited comparable sensitivity (mean IC_{50} = 19 µM), whereas OCI-AML3, Kasumi1 or M07E showed impaired or incomplete responses (IC_{50}: OCI-AML3: 32 µM, Kasumi-1/M07e: NM = not measurable; Fig. 5b and Supplementary Fig. 5c).

Importantly, DCZ0415 treatment resulted in activation of the TP53 pathway and cell death, effects that were rescued by enforced TRIP13 expression or by *Trp53* deletion (Fig. 5c, Supplementary Fig. 5d and Supplementary Table 5), confirming on-target activity and TP53-dependent mechanisms of action.

Consistent with the *in vitro* findings, *in vivo* fluorescence-based competitive transplantation assays demonstrated marked depletion of *Trip13*-deficient fetal NUP98::KDM5A$^+$ blasts in the bone marrow of recipient mice at the experimental endpoint (Fig. 5d-e).

526 Together, these data demonstrate that pharmacologic inhibition of TRIP13 reactivates
527 TP53 signaling and selectively compromises the survival of NUP98::KDM5A⁺ leukemic
528 cells, providing functional proof-of-concept that TRIP13 represents a therapeutically
529 targetable vulnerability in this high-risk pediatric AML subtype.

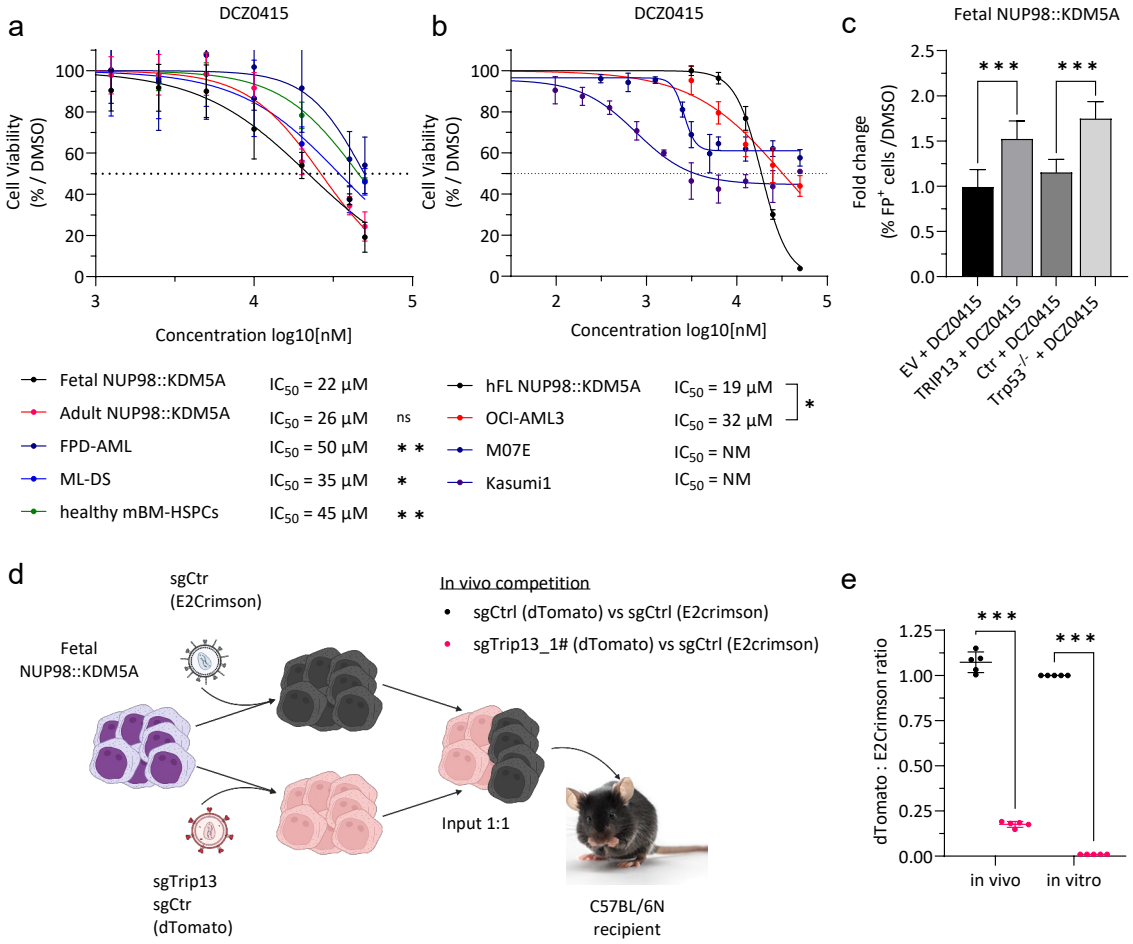

530

531 **Fig. 5. Pharmacological inhibition of the TRIP13-TP53 axis is a therapeutic option for**
532 **NUP98::KDM5A⁺ pediatric leukemia.**

533 a) Dose-response curves for DCZ0415 (TRIP13 inhibitor) in fetal and adult NUP98::KDM5A⁺,
534 ML-DS and FPD-AML models and healthy mBM-HSPCs after 5 days of treatment *in vitro*.
535 The corresponding IC_{50}-values are depicted below the graphs. (mean ± s.d. , n > 3, 1-way
536 ANOVA related to fetal NUP98::KDM5A⁺ cells)

537 b) Dose-response curves for DCZ0415 (TRIP13 inhibitor) in hFL NUP98::KDM5A⁺ cells and
538 OCI-AML3, M07E and Kasumi1 after 5 days of treatment *in vitro*. The corresponding IC_{50}-
539 values are depicted below the graphs. (mean ± s.d. , n > 3, 1-way ANOVA related to hFL
540 NUP98::KDM5A⁺ cells)

541 c) Bar graphs showing the percentage of sgRNA-transduced (negative control sgRNA [sgCtr],
542 sgTrp53) and empty vector (EV) or TRIP13-overexpressing fetal NUP98::KDM5A$^+$ cells
543 after 7 days of treatment with DCZ0415 (TRIP13 inhibitor) *in vitro*. (mean±s.d. , n > 3, 1-
544 way ANOVA)
545 d) Experimental setup for evaluating the genetic ablation of *Trip13* in fetal NUP98::KDM5A$^+$
546 cells *in vivo*. Fetal NUP98::KDM5A$^+$ cells (with stable Cas9 expression) were co-
547 transduced with sgTrip13 (dTomato) and sgCtr (dTomato) and mixed 1:1 with sgCtr
548 (E2Crimson), before transplantation into sublethally irradiated recipient mice.
549 e) Dot plot showing the ratio of dTomato$^+$ to E2Crimson$^+$ cells in the bone marrow of mice
550 euthanized 4 weeks after transplantation (n = 5) and after 4 weeks of culture, normalized
551 to day 0 (n = 3, 2-way ANOVA).
552 ns, not significant * P < .05, ** P < .01, ***P < .001, ****P < .0001.

553 # Discussion

554 In this study, we adopted a developmental perspective to leukemogenesis to uncover
555 a previously unrecognized vulnerability in pediatric NUP98::KDM5A$^+$ AML. Rather than
556 focusing exclusively on oncogenic lesions, we interrogated how fetal versus adult
557 hematopoietic contexts shape leukemic behavior and dependencies. This ontogeny-
558 centered approach revealed a developmentally restricted survival axis centered on
559 TP53 suppression and establishes a conceptual framework that may extend to other
560 malignancies with strong developmental origins.
561 NUP98::KDM5A-rearranged AML is a rare but highly aggressive leukemia that occurs
562 predominantly in infants and very young children below the age of 2 years [6-8], with
563 clinical and genomic evidence supporting leukemic initiation during embryogenesis
564 [52]. Despite intensive chemotherapy and allogeneic hematopoietic stem cell
565 transplantation (HSCT), outcomes remain poor, relapses are frequent, and treatment-
566 related morbidity is substantial. Achieving deep, measurable residual disease (MRD)–
567 negative remissions before HSCT is crucial for long-term survival, yet current induction
568 regimens are often too toxic or insufficiently effective in this fragile patient population

569 [53]. These challenges underscore the need for biologically informed, mechanism-
570 based therapeutic strategies tailored to the unique features of infant AML.
571 Ontogeny has emerged as a critical modifier of disease biology in several pediatric
572 leukemias, including CBFA2T3::GLIS2- and KMT2A-rearranged AML [6]. However, its
573 role in NUP98::KDM5A-driven leukemia has not been directly addressed. Using
574 matched fetal and adult HSPC models, we demonstrate that NUP98::KDM5A-driven
575 leukemia arising in a fetal context is more aggressive and retains fetal-specific
576 transcriptional programs [22, 23, 54]. Functional genomic interrogation of fetal-
577 enriched genes identified *TRIP13*, a AAA^+ ATPase and direct interactor of the TP53
578 phosphatase PPM1D/WIP1, as a critical dependency in fetal NUP98::$KDM5A^+$ cells.
579 Mechanistically, our data show that TRIP13 suppresses TP53 pathway activation and
580 that its genetic or pharmacologic inhibition leads to robust TP53 activation, G_2/M arrest
581 and mitochondrial apoptosis without additional accumulation of DNA damage [45, 46].
582 These data support a model in which TRIP13 mitigates NUP98::KDM5A-induced DNA
583 stress [55] by modulating TP53 activity, at least in part through its physical interaction
584 with PPM1D, a well-established oncogenic suppressor of TP53 [56]. While the precise
585 molecular mechanism by which TRIP13 regulates PPM1D activity remains to be
586 elucidated, the ATPase-dependent capacity of TRIP13 to remodel protein complexes
587 [57] raises the possibility that it modulates PPM1D conformation, thereby fine-tuning
588 TP53 signaling. Notably, the broader TRIP13 interactome includes multiple TP53
589 network components, likely accounting for the more pronounced TP53 activation
590 observed upon *TRIP13* loss compared with *PPM1D* deletion alone.
591 Consistent with this developmental model, our functional screens also identified
592 dependencies on oncofetal regulators previously reported as direct NUP98::KDM5A
593 targets, such as *Igf2bp3* [55, 58], supporting the notion that this fusion sustains
594 leukemic maintenance in part through enforcement of fetal gene expression programs.

595 Our findings complement prior studies identifying transcriptional and cell-cycle
596 dependencies in NUP98::KDM5A-driven leukemia, including the MEN–KMT2A axis,
597 CDK6, and CDK12 [54, 55, 58]. These dependencies converge on sustained
598 proliferation and transcriptional output, processes inherently associated with replicative
599 stress and DNA damage [59]. In line with these observations, NUP98::KDM5A-
600 expressing cells exhibit a marked baseline DNA damage, reliance on DNA damage
601 response pathways, and heightened sensitivity to CDK12/13 inhibition [55, 60]. Our
602 work adds an essential layer to this model by demonstrating that leukemic survival
603 under such stress conditions requires active control of TP53-mediated apoptosis
604 through a TRIP13-centered mechanism. The overlap between DNA damage-
605 associated genes identified in our screens and those reported to be maintained and
606 upregulated by NUP98::KDM5A during fetal development [55], further supports this
607 integrated model.
608 Importantly, we provide proof-of-concept that TRIP13 is pharmacologically targetable.
609 The small-molecule inhibitor DCZ0415 faithfully recapitulated the effects of genetic
610 *TRIP13* loss by inducing TP53-dependent apoptosis in NUP98::KDM5A^{+} AML cells,
611 and *Trip13*-depleted cells were selectively impaired *in vivo*. Although DCZ0415 has
612 not yet been evaluated clinically, these data validate TRIP13 as a druggable node and
613 provide a strong rationale for the development of next-generation TRIP13 inhibitors
614 with improved potency and pharmacologic properties suitable for clinical evaluation.
615 Beyond identifying TRIP13 as a therapeutic target, our TP53-pathway CRISPR screen
616 delineated genetic modifiers that shape the cellular response to TP53 reactivation.
617 Resistance to *TRIP13* loss was conferred by disruption of core apoptotic mediators
618 such as *TP53*, *CHEK2*, *BAX*, and *BBC3/PUMA*, establishing mitochondrial apoptosis
619 as the dominant execution pathway. Conversely, enhanced sensitivity to *TRIP13* loss
620 was observed upon perturbation of cell-cycle and transcriptional regulators, including

621 *CDK1*, *CDK4*, *CDK9*, and *HDAC1*, highlighting conditional co-dependencies emerging
622 under TRIP13-loss induced TP53 signaling. Together, these interactions further
623 underscore the central role of TP53 suppression in sustaining fetal NUP98::KDM5A-
624 driven leukemic survival.
625 More broadly, our study illustrates how systematic functional interrogation of
626 developmental programs can reveal age- and lineage-specific vulnerabilities that are
627 not apparent from mutation-focused analyses alone. In NUP98::KDM5A^{+} AML, this
628 strategy uncovered a developmentally constrained TRIP13–PPM1D–TP53 survival
629 axis that is essential for leukemic maintenance and therapeutically exploitable.
630 Leveraging developmental biology to expose such context-specific dependencies may
631 represent a powerful paradigm for identifying novel targets in other aggressive
632 pediatric cancers with a clear developmental origin.

633 Acknowledgments

634 The authors thank D. Trono of EPFL (Lausanne, Switzerland), for kindly providing both
635 pMD2.G (plasmid 12259; Addgene) and psPAX2 (plasmid 12260; Addgene); A. Santos
636 (University of Halle-Wittenberg) for assistance with flow cytometry; and K. Huke for
637 assistance with animal experiments. The authors thank C. Hugenberg for assistance
638 and proofreading.

639 **Funding:** L.N.C., M.V., and D.H. were supported by the Frankfurt Foundation for
640 Children with Cancer. This work was supported by the German José Carreras
641 Leukemia Foundation (DJCLS 12 R/2024) and by grants from the parents' Association
642 "Hilfe für Krebskranke Kinder e.V." (C^{3}OMBAT-AML, L.N.C., J.H.K. and D.H)., the
643 European Research Council Horizon 2020 program (#714226), and the German
644 Research Foundation (DFG; FOR 5433 RNA in Focus; KL-2371/7).

Illustrations (Figures 1a, 2a, 4a and 5d and graphical abstract; https://BioRender.com/3to2ktx, https://BioRender.com/q0hsqlg, https://BioRender.com/qo23x2o, https://BioRender.com/3q2on7c, https://biorender.com/94pt6jg) were created in BioRender.com.

Contributions

L.N.C. performed experiments, analyzed and interpreted the data, and wrote the manuscript; L.P., H.I., and C.I. performed experiments, analyzed the data, and revised the manuscript; K.S. performed bioinformatics analysis and revised the manuscript; K.M., and L.G. performed experiments; M.V. revised the manuscript; A.S. supervised the analyses and revised the manuscript; D.H. and J.H.K designed the study, analyzed and interpreted the data, wrote the manuscript, and academically drove the project.

Disclosures: J.H.K has advisory roles for Boehringer, Roche and Jazz Pharmaceuticals. All other authors declare that the manuscript was written in the absence of any commercial or financial relationships that could be perceived as a potential conflict of interest.

Correspondence: Prof. Dr. Dirk Heckl, Institute for Experimental Pediatric Hematology and Oncology, Goethe-University Frankfurt, Komturstrasse 3a, 60528 Frankfurt am Main, Germany; e-mail: heckl@med.uni-frankfurt.de.

Availability of data and materials

RNA-seq gene expression data have been deposited in the National Center for Biotechnology Information's Gene Expression Omnibus (accession numbers GSE308953, GSE308954, and GSE308955).

667 # References

668 1. Bolouri, H., et al., *The molecular landscape of pediatric acute myeloid leukemia reveals*
669 *recurrent structural alterations and age-specific mutational interactions.* Nat Med, 2018. **24**(1):
670 p. 103-112.
671 2. Papaemmanuil, E., et al., *Genomic Classification and Prognosis in Acute Myeloid Leukemia.* N
672 Engl J Med, 2016. **374**(23): p. 2209-2221.
673 3. Marceau-Renaut, A., et al., *Molecular Profiling Defines Distinct Prognostic Subgroups in*
674 *Childhood AML: A Report From the French ELAM02 Study Group.* Hemasphere, 2018. **2**(1): p.
675 e31.
676 4. Reinhardt, D., E. Antoniou, and K. Waack, *Pediatric Acute Myeloid Leukemia-Past, Present, and*
677 *Future.* J Clin Med, 2022. **11**(3).
678 5. Elgarten, C.W. and R. Aplenc, *Pediatric acute myeloid leukemia: updates on biology, risk*
679 *stratification, and therapy.* Current Opinion in Pediatrics, 2020. **32**(1): p. 57-66.
680 6. Lopez, C.K., et al., *Ontogenic Changes in Hematopoietic Hierarchy Determine Pediatric*
681 *Specificity and Disease Phenotype in Fusion Oncogene-Driven Myeloid Leukemia.* Cancer
682 Discov, 2019. **9**(12): p. 1736-1753.
683 7. Okeyo-Owuor, T., et al., *The efficiency of murine MLL-ENL-driven leukemia initiation changes*
684 *with age and peaks during neonatal development.* Blood Adv, 2019. **3**(15): p. 2388-2399.
685 8. Calvi, L.M. and D.C. Link, *The hematopoietic stem cell niche in homeostasis and disease.* Blood,
686 2015. **126**(22): p. 2443-51.
687 9. Mack, R., et al., *The Fetal-to-Adult Hematopoietic Stem Cell Transition and its Role in Childhood*
688 *Hematopoietic Malignancies.* Stem Cell Rev Rep, 2021. **17**(6): p. 2059-2080.
689 10. de Smith, A.J. and L.G. Spector, *In Utero Origins of Acute Leukemia in Children.* Biomedicines,
690 2024. **12**(1).
691 11. Gruber, T.A. and J.R. Downing, *The biology of pediatric acute megakaryoblastic leukemia.*
692 Blood, 2015. **126**(8): p. 943-9.
693 12. de Rooij, J.D., et al., *Pediatric non-Down syndrome acute megakaryoblastic leukemia is*
694 *characterized by distinct genomic subsets with varying outcomes.* Nat Genet, 2017. **49**(3): p.
695 451-456.
696 13. de Rooij, J.D., et al., *Recurrent abnormalities can be used for risk group stratification in*
697 *pediatric AMKL: a retrospective intergroup study.* Blood, 2016. **127**(26): p. 3424-30.
698 14. Gough, S.M., C.I. Slape, and P.D. Aplan, *NUP98 gene fusions and hematopoietic malignancies:*
699 *common themes and new biologic insights.* Blood, 2011. **118**(24): p. 6247-57.
700 15. Bertrums, E.J.M., et al., *Comprehensive molecular and clinical characterization of NUP98*
701 *fusions in pediatric acute myeloid leukemia.* Haematologica, 2023.
702 16. Gough, S.M., et al., *NUP98-PHF23 is a chromatin-modifying oncoprotein that causes a wide*
703 *array of leukemias sensitive to inhibition of PHD histone reader function.* Cancer Discov, 2014.
704 **4**(5): p. 564-77.
705 17. Wang, G.G., et al., *Haematopoietic malignancies caused by dysregulation of a chromatin-*
706 *binding PHD finger.* Nature, 2009. **459**(7248): p. 847-51.
707 18. Wang, G.G., et al., *NUP98-NSD1 links H3K36 methylation to Hox-A gene activation and*
708 *leukaemogenesis.* Nat Cell Biol, 2007. **9**(7): p. 804-12.
709 19. Bowie, M.B., et al., *Identification of a new intrinsically timed developmental checkpoint that*
710 *reprograms key hematopoietic stem cell properties.* Proc Natl Acad Sci U S A, 2007. **104**(14): p.
711 5878-82.
712 20. Popescu, D.M., et al., *Decoding human fetal liver haematopoiesis.* Nature, 2019. **574**(7778): p.
713 365-371.
714 21. Ranzoni, A.M., et al., *Integrative Single-Cell RNA-Seq and ATAC-Seq Analysis of Human*
715 *Developmental Hematopoiesis.* Cell Stem Cell, 2021. **28**(3): p. 472-487.e7.

716 22. Roy, A., et al., *Transitions in lineage specification and gene regulatory networks in*
717 *hematopoietic stem/progenitor cells over human development.* Cell Rep, 2021. **36**(11): p.
718 109698.
719 23. Ivanovs, A., et al., *Human haematopoietic stem cell development: from the embryo to the dish.*
720 Development, 2017. **144**(13): p. 2323-2337.
721 24. Gialesaki, S., et al., *RUNX1 isoform disequilibrium promotes the development of trisomy 21–*
722 *associated myeloid leukemia.* Blood, 2023. **141**(10): p. 1105-1118.
723 25. Alejo-Valle, O., et al., *The megakaryocytic transcription factor ARID3A suppresses leukemia*
724 *pathogenesis.* Blood, 2022. **139**(5): p. 651-665.
725 26. Emmrich, S., et al., *miR-99a/100~125b tricistrons regulate hematopoietic stem and progenitor*
726 *cell homeostasis by shifting the balance between TGFβ and Wnt signaling.* Genes Dev, 2014.
727 **28**(8): p. 858-74.
728 27. Bhayadia, R., et al., *Endogenous Tumor Suppressor microRNA-193b: Therapeutic and*
729 *Prognostic Value in Acute Myeloid Leukemia.* J Clin Oncol, 2018. **36**(10): p. 1007-1016.
730 28. Labuhn, M., et al., *Refined sgRNA efficacy prediction improves large- and small-scale CRISPR-*
731 *Cas9 applications.* Nucleic Acids Res, 2018. **46**(3): p. 1375-1385.
732 29. Reimer, J., et al., *CRISPR-Cas9-induced t(11;19)/MLL-ENL translocations initiate leukemia in*
733 *human hematopoietic progenitor cells in vivo.* Haematologica, 2017. **102**(9): p. 1558-1566.
734 30. de Rooij, J.D., et al., *NUP98/JARID1A is a novel recurrent abnormality in pediatric acute*
735 *megakaryoblastic leukemia with a distinct HOX gene expression pattern.* Leukemia, 2013.
736 **27**(12): p. 2280-8.
737 31. Labuhn, M., et al., *Mechanisms of Progression of Myeloid Preleukemia to Transformed Myeloid*
738 *Leukemia in Children with Down Syndrome.* Cancer Cell, 2019. **36**(2): p. 123-138.e10.
739 32. Li, W., et al., *MAGeCK enables robust identification of essential genes from genome-scale*
740 *CRISPR/Cas9 knockout screens.* Genome Biol, 2014. **15**(12): p. 554.
741 33. Ianevski, A., A.K. Giri, and T. Aittokallio, *SynergyFinder 3.0: an interactive analysis and*
742 *consensus interpretation of multi-drug synergies across multiple samples.* Nucleic Acids
743 Research, 2022. **50**(W1): p. W739-W743.
744 34. Chen, S., et al., *fastp: an ultra-fast all-in-one FASTQ preprocessor.* Bioinformatics, 2018. **34**(17):
745 p. i884-i890.
746 35. Spinozzi, G., et al., *ARPIR: automatic RNA-Seq pipelines with interactive report.* BMC
747 Bioinformatics, 2020. **21**(Suppl 19): p. 574.
748 36. Love, M.I., W. Huber, and S. Anders, *Moderated estimation of fold change and dispersion for*
749 *RNA-seq data with DESeq2.* Genome Biol, 2014. **15**(12): p. 550.
750 37. Benjamini, Y. and Y. Hochberg, *Controlling the False Discovery Rate: A Practical and Powerful*
751 *Approach to Multiple Testing.* Journal of the Royal Statistical Society: Series B
752 (Methodological), 1995. **57**(1): p. 289-300.
753 38. Subramanian, A., et al., *Gene set enrichment analysis: A knowledge-based approach for*
754 *interpreting genome-wide expression profiles.* Proceedings of the National Academy of
755 Sciences, 2005. **102**(43): p. 15545-15550.
756 39. Mootha, V.K., et al., *PGC-1α-responsive genes involved in oxidative phosphorylation are*
757 *coordinately downregulated in human diabetes.* Nature Genetics, 2003. **34**(3): p. 267-273.
758 40. Harrison, P.W., et al., *Ensembl 2024.* Nucleic Acids Research, 2023. **52**(D1): p. D891-D899.
759 41. Noort, S., et al., *The clinical and biological characteristics of NUP98-KDM5A in pediatric acute*
760 *myeloid leukemia.* Haematologica, 2021. **106**(2): p. 630-634.
761 42. Schwarzer, A., et al., *The non-coding RNA landscape of human hematopoiesis and leukemia.*
762 Nat Commun, 2017. **8**(1): p. 218.
763 43. Förster, A., et al., *Beyond Pathogenic RUNX1 Germline Variants: The Spectrum of Somatic*
764 *Alterations in RUNX1-Familial Platelet Disorder with Predisposition to Hematologic*
765 *Malignancies.* Cancers (Basel), 2022. **14**(14).
766 44. Grimm, J., D. Heckl, and J.H. Klusmann, *Molecular Mechanisms of the Genetic Predisposition*
767 *to Acute Megakaryoblastic Leukemia in Infants With Down Syndrome.* Front Oncol, 2021. **11**:
768 p. 636633.

769 45. Vader, G., *Pch2TRIP13: controlling cell division through regulation of HORMA domains.*
770 Chromosoma, 2015. **124**(3): p. 333-339.
771 46. Banerjee, R., et al., *TRIP13 promotes error-prone nonhomologous end joining and induces*
772 *chemoresistance in head and neck cancer.* Nat Commun, 2014. **5**: p. 4527.
773 47. Jeong, H., et al., *TRIP13 Participates in Immediate-Early Sensing of DNA Strand Breaks and ATM*
774 *Signaling Amplification through MRE11.* Cells, 2022. **11**(24).
775 48. Sullivan, K.D., et al., *Mechanisms of transcriptional regulation by p53.* Cell Death &
776 Differentiation, 2018. **25**(1): p. 133-143.
777 49. Kruse, J.-P. and W. Gu, *Modes of p53 Regulation.* Cell, 2009. **137**(4): p. 609-622.
778 50. Andrysik, Z., et al., *PPM1D suppresses p53-dependent transactivation and cell death by*
779 *inhibiting the Integrated Stress Response.* Nat Commun, 2022. **13**(1): p. 7400.
780 51. Wang, Y., et al., *A Small-Molecule Inhibitor Targeting TRIP13 Suppresses Multiple Myeloma*
781 *Progression.* Cancer Res, 2020. **80**(3): p. 536-548.
782 52. Cazzola, A., et al., *Prenatal Origin of Pediatric Leukemia: Lessons From Hematopoietic*
783 *Development.* Front Cell Dev Biol, 2020. **8**: p. 618164.
784 53. Rettinger, E., et al., *The hallmarks of hematopoietic stem cell transplantation for pediatric*
785 *acute myeloid leukemia.* Leukemia, 2025.
786 54. Heikamp, E.B., et al., *The menin-MLL1 interaction is a molecular dependency in NUP98-*
787 *rearranged AML.* Blood, 2022. **139**(6): p. 894-906.
788 55. Troester, S., et al., *Transcriptional and epigenetic rewiring by the NUP98::KDM5A fusion*
789 *oncoprotein directly activates CDK12.* Nat Commun, 2025. **16**(1): p. 4656.
790 56. Ogasawara, S., et al., *Novel inhibitors targeting PPM1D phosphatase potently suppress cancer*
791 *cell proliferation.* Bioorg Med Chem, 2015. **23**(19): p. 6246-9.
792 57. Mapelli, M. and A. Musacchio, *MAD contortions: conformational dimerization boosts spindle*
793 *checkpoint signaling.* Curr Opin Struct Biol, 2007. **17**(6): p. 716-25.
794 58. Schmoellerl, J., et al., *CDK6 is an essential direct target of NUP98 fusion proteins in acute*
795 *myeloid leukemia.* Blood, 2020. **136**(4): p. 387-400.
796 59. Shimura, T., et al., *Cyclin D1 overexpression perturbs DNA replication and induces replication-*
797 *associated DNA double-strand breaks in acquired radioresistant cells.* Cell Cycle, 2013. **12**(5):
798 p. 773-82.
799 60. Domingo-Reinés, J., et al., *The pediatric leukemia oncoprotein NUP98-KDM5A induces genomic*
800 *instability that may facilitate malignant transformation.* Cell Death Dis, 2023. **14**(6): p. 357.

801